CHAOS **21**, 033113 (2011)

Nonlinear vocal fold dynamics resulting from asymmetric fluid loading on a two-mass model of speech

Byron D. Erath,[1,a)] Matías Zañartu,[2] Sean D. Peterson,[3] and Michael W. Plesniak[1]
[1]*Department of Mechanical and Aerospace Engineering, The George Washington University, Washington DC 20052, USA*
[2]*Department of Electronic Engineering, Universidad Técnica Federico Santa María, Valparaíso, Chile 2390123*
[3]*Department of Mechanical and Mechatronics Engineering, University of Waterloo, Waterloo, Ontario N2L 3G1, Canada*

(Received 23 February 2011; accepted 7 July 2011; published online 22 August 2011)

Nonlinear vocal fold dynamics arising from asymmetric flow formations within the glottis are investigated using a two-mass model of speech with asymmetric vocal fold tensioning, representative of unilateral vocal fold paralysis. A refined theoretical boundary-layer flow solver is implemented to compute the intraglottal pressures, providing a more realistic description of the flow than the standard one-dimensional, inviscid Bernoulli flow solution. Vocal fold dynamics are investigated for subglottal pressures of $0.6 < p_s < 1.5$ kPa and tension asymmetries of $0.5 < Q < 0.8$. As tension asymmetries become pronounced the asymmetric flow incites nonlinear behavior in the vocal fold dynamics at subglottal pressures that are associated with normal speech, behavior that is not captured with standard Bernoulli flow solvers. Regions of bifurcation, coexistence of solutions, and chaos are identified. © *2011 American Institute of Physics*. [doi:10.1063/1.3615726]

Understanding the nature of nonlinear behavior in normal and disordered voice has an impact on behavioral, clinical, and technological aspects of speech science. Models that can mimic and predict these phenomena have been shown to be useful tools for investigation, diagnosis, and treatment of vocal maladies. Simplified lumped element models of the vocal folds have received significant attention due to their ability to efficiently perform comprehensive parameter variation investigations, a necessary task that becomes prohibitive with more advanced computational models. However, the limiting assumptions of these models often prevent them from replicating complicated speech behaviors. In this study, a compact physics-based asymmetric flow solution replaces the traditionally simplistic Bernoulli flow equation to compute the aerodynamic loadings that drive the model vocal fold motion. The new, more comprehensive flow model is used to extend previous chaotic descriptions obtained using advanced flow solvers for a limited set of conditions representative of unilateral paralysis. It is shown that asymmetric intraglottal flow incites chaotic vocal fold motion in the pressure-imbalance bifurcation space at more common physiological conditions, thus increasing the chances of encountering chaos in disordered speech.

I. INTRODUCTION

Various experimental methodologies exist for the investigation of pathological voice conditions, with lumped-element models of speech being some of the most ubiquitous. Their relative simplicity and inexpensive computational cost enables them to be used for broad parametric investigations of behaviors found in both normal and disordered speech. The model presented by Steinecke and Herzel[25] (SH) is one of the most prevalent, as it has been used to benchmark analysis tools[33,41] and its behavior has been related to excised larynx experiments,[11,29,34,41] irregularities in normal voices,[16] and a variety of pathological conditions including paralysis,[11,25,28,30] Parkinsonian voice,[39] vocal tremor,[40] and breathiness.[12]

The ability of all lumped-element models to replicate common phonatory conditions relies on a number of parameters. The prescription of the fluid loading that imparts energy to the system and drives the vocal fold (VF) motion is a key component. In virtually all multi-mass models of speech, the aerodynamics are modeled using a simple Bernoulli flow solver that assumes symmetric, invsicid, 1D flow. A notable exception includes the development of a flow solver that incorporates boundary layer effects, and a varying flow separation point.[21] However, this flow solver also assumes a symmetric flow orientation within the glottis. In contrast, experimental data reveal that during the closing phases of the vocal fold cycle, when the glottis is divergent, complex viscous flow behavior arises, characterized by asymmetric flow attachment to the vocal fold walls, unsteady flow separation, vortex shedding, and transition to turbulence.[2,6,8,18,27]

More detailed modeling of the flow behavior has been provided by Tao and Jiang,[28,30] who coupled a computational fluid dynamics (CFD) flow solver with the two-mass model (2MM) of SH.[25] Although the inclusion of a full CFD solver counteracts the appeal of the efficient and cost-effective lumped element approach, the advanced complexity of the CFD flow solver highlighted the need for more realistic multi-mass flow solvers. It was found that the fully-coupled CFD solver incited chaotic motion in the 2MM vocal fold dynamics for subglottal pressures that were associated with normal speech,[28,30] as opposed to prior work that only observed the onset of chaotic motion at

---

[a] Electronic mail: erath@gwu.edu.

unrealistically high subglottal pressures.[16,25] Unfortunately, the limited range of CFD investigations prevented a complete understanding of the role of asymmetric fluid loadings over a broad range of subglottal pressures and tissue asymmetries.

Recently, Erath *et al.*[3] developed a novel, physics-based flow solver derived from boundary layer theory to describe asymmetric flow attachment within the divergent glottis. Easily incorporated into any lumped element model, this theoretical flow solution generates a simple algebraic description of the asymmetric intraglottal pressures that arise from the flow physics, and ultimately drive the vocal fold motion. The solution can be seamlessly integrated into existing codes for multi-mass speech models, allowing quick, efficient investigations of asymmetric flow behavior in a variety of pathological conditions. Because the refined flow solver only models the development of asymmetric intraglottal flows, neglecting vortex shedding and flow transition to turbulence, it facilitates identification of the specific traits of vocal fold dynamics that arise due to asymmetric flow attachment within the glottis.

This paper seeks to elucidate the influence of asymmetric flow loading on the vocal folds under pathological conditions representative of unilateral paralysis. The genesis of nonlinear behavior arising from the refined flow solver is investigated over a wide range of subglottal pressures and asymmetry conditions that are encountered for both normal and pathological speech conditions. Comparisons of the vocal fold dynamics resulting from the compact asymmetric flow solution are made to those generated from the Bernoulli and fully-coupled CFD flow simulations. In these investigations, nonlinear analysis tools are used to elucidate irregular behavior where standard linear analysis techniques may fail.[15] These methods are gaining importance in speech science and show promise as clinical techniques for improved identification of various vocal pathologies.[11,13,14,35,38]

II. NUMERICAL METHODS AND ANALYSIS

A. Numerical Two-Mass Model

Steinecke and Herzel[25] developed a 2MM of speech that enables tension asymmetries to be prescribed for the opposing vocal folds. The SH model represents each vocal fold as two coupled spring-mass-dampers. Figure 1 shows the relevant parameters of the model. Although the SH model is a simplified view of vocal fold geometry, its ubiquity and relevance in the speech literature renders it an ideal candidate for modification and comparison purposes.

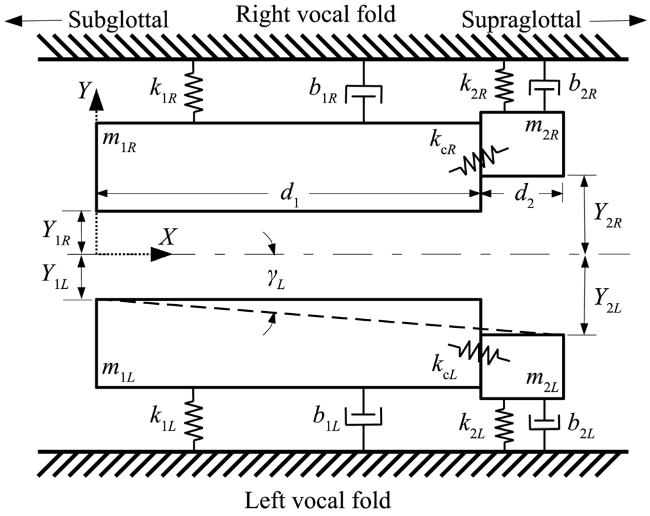

FIG. 1. Schematic diagram of the two-mass model configuration and parameters.

The orientations of the vocal folds are denoted by two subscripts, j and α, where $j = 1$ and 2, and identifies the inferior and superior (subglottal and supraglottal) positions of the masses, respectively. The second subscript, $\alpha = L$ and R, denotes the left and the right vocal fold, respectively. Masses are denoted as $m_{j\alpha}$, spring constants are $k_{j\alpha}$, and damping constants are $b_{j\alpha}$, with the spring and damping coefficients describing the tissue properties. The masses on each side are coupled together with a spring $k_{c\alpha}$, where the subscript c is a dummy index that merely identifies the coupling spring constant.

The governing equations for the vocal fold motion are

$$m_{1\alpha}\ddot{Y}_{1\alpha} + b_{1\alpha}\dot{Y}_{1\alpha} + k_{1\alpha}Y_{1\alpha} + \Theta(-a_1)\frac{c_{1\alpha}a_1}{2l} + k_{c\alpha}(Y_{1\alpha} - Y_{2\alpha}) = G(t) \tag{1a}$$

$$m_{2\alpha}\ddot{Y}_{2\alpha} + b_{2\alpha}\dot{Y}_{2\alpha} + k_{2\alpha}Y_{2\alpha} + \Theta(-a_2)\frac{c_{2\alpha}a_2}{2l} + k_{c\alpha}(Y_{2\alpha} - Y_{1\alpha}) = 0, \tag{1b}$$

where $Y_{j\alpha}$ is the displacement of the mass from the glottal midline (as shown in Fig. 1), with a dot over the variable indicating differentiation with respect to time t. Additional springs with constants $c_{j\alpha}$ (not shown in Fig. 1) model the impact forces that occur during vocal fold collision, and are modulated by the Heaviside function, Θ, such that they are only activated when the area between the vocal fold masses $a_j < 0$. All simulations are computed for 600 ms using a Runge-Kutta solver with a step size that corresponds to a sampling frequency of $f_s = 20$ kHz. The total length of the vocal folds in the anterior/posterior direction (into the page in Fig. 1) is l. Finally, $G(t)$ is a time-varying forcing function resulting from the aerodynamic loading that drives the vocal fold motion. Following the implementation of SH, the forcing function is only applied to the inferior masses. The forcing can be further decomposed into opening and closing phase components, $G = G_{\text{open}} + G_{\alpha,\text{close}}$. Note that the closing phase has a wall (α) dependency that will be discussed later. The aerodynamic loading during the opening phase is driven by the subglottal pressure, p_s. Because the glottis forms a convergent channel, during the opening phase, the pressure gradient is favorable, and the boundary layers are thin, allowing the aerodynamic loadings to be approximated by the Bernoulli equation as

$$G_{\text{open}} = ld_1p_1 = ld_1p_s\left[1 - \left(\frac{a_{\min}}{a_1}\right)^2\right]\Theta(a_1)\Theta(\gamma_{\text{tot}}), \tag{2}$$

where d_1 is the length of the inferior masses in the X direction, and $a_{\min}$ is the minimum glottal area, defined as

$$a_{\min} = \max(0, \min(a_1, a_2)). \tag{3}$$

The total included angle of the two vocal folds is specified as γ_{tot}, see Fig. 1. Due to the limiting nature of the function Θ, the opening force, G_{open}, is zero when the glottis forms a uniform or divergent channel.

Virtually all flow solutions implemented into multi-mass model investigations of speech assume highly-idealized 1D, symmetric, inviscid flow throughout the entire phonatory cycle. The standard SH implementation specifies that when the glottis forms a divergent channel, the flow symmetrically separates at the minimal glottal diameter. Consequently, $G_{\text{close}} = 0$, and there is no force applied to either of the vocal fold walls during the closing phases of the cycle. These simplified flow models are incapable of modeling important flow asymmetries that develop during the divergent portion of the phonatory cycle. In response to this deficiency, Erath *et al.*[3] developed a new theoretical flow solver using a boundary layer estimation of the asymmetric pressure (BLEAP). This model is predicated on experimental and numerical observations that the glottal jet attaches to one vocal fold wall when the glottis forms a divergent channel.[6,7,18,22,27,33]

In short, the medial vocal fold surfaces are modeled as two translating and rotating semi-infinite flat plates, where it is assumed that the flow is fully-attached to one plate, and fully-separated from the opposing one (non-flow wall). The pressure distribution along the non-flow wall is assumed to be constant and equal to the supraglottal pressure. The pressure along the flow wall is found by approximating the flow field as a boundary layer and solving the governing equations using similarity analysis.[10]

As discussed by Erath *et al.*,[3] the plate translation does not significantly influence the pressure distribution along the flow wall. The wall rotation, however, acts as a favorable pressure gradient, regardless of the direction of rotation. Solving the boundary layer equations in a rotating reference frame, the pressure distribution along the flow wall can be estimated as

$$p(x) = p_i + \frac{1}{2}\rho(u_i^2 - u(x)^2), \tag{4}$$

where p_i and u_i are the pressure and velocity at the inlet of the glottis, respectively, $x_e = d_1 + d_2$ is the length of the vocal fold wall, and $u(x)$ is the velocity at the edge of the boundary layer. The pressure at the glottal inlet is given by

$$p_i = \frac{1}{2}\rho u_i^2\left(\left(\frac{x_e + x_{\text{off}}}{x_{\text{off}}}\right)^{2b} - 1\right). \tag{5}$$

with

$$u_i = \sqrt{\frac{2p_s}{\rho}}\left(\frac{x_{\text{off}}}{x_e + x_{\text{off}}}\right)^b \tag{6}$$

and

$$u(x) = u_i\left(\frac{x + x_{\text{off}}}{x_{\text{off}}}\right)^b. \tag{7}$$

In order to satisfy the similarity solution the velocity must develop as a power-law relation, where b is the exponent. The theoretical solution very closely matches experimental data for values of $b = -0.015$ and $x_{\text{off}} = 0.2$ mm.[3] The variable x_{off} is an experimentally-measured value that is introduced to ensure the theoretical boundary layer has a finite height at the glottal inlet. The result of Eq. (4) produces a physically-realistic description of the flow (asymmetric attachment to one wall, with complete separation from the opposing wall) in a compact, algebraic relation that is easily incorporated into existing 2MM fluid flow solvers.

For the case of asymmetric flow attachment to one wall the closing force $G_{\alpha,\text{close}}$ is defined as

$$G_{\alpha,\text{close}} = \Theta(a_{\min})\Theta(-\gamma)\int_0^{x_e} p(x)dx, \tag{8}$$

where $p(x)$ is obtained from Eq. (4). The subscript α denotes the wall to which the flow is attached. This is determined during the computation by specifying that the flow attaches to the vocal fold wall that has the shallower divergence angle (more positive) when the total divergence angle γ_{tot} becomes negative. The preference of the flow to repeatedly attach to the shallower-angled wall has been established with experimental investigations.[4–6] Once the flow attaches to one wall in the numerical model, it remains attached until either $\gamma_{\text{tot}} > 0$, or $a_{\min} = 0$.

B. Time Series and Non-linear Analysis

The 2MM of SH is useful for investigating speech pathologies, including superior laryngeal nerve (SLN) paralysis.[25] Tension imbalance is modeled by defining a symmetry parameter, $0 < Q < 1.0$, such that

$$\begin{aligned} m_{j,R} &= m_{j,L}/Q, \quad k_{j,R} = Qk_{j,L}, \\ k_{c,R} &= Qk_{c,L}, \quad c_{j,R} = Qc_{j,L}. \end{aligned} \tag{9}$$

When $Q = 1.0$ vocal fold tension is perfectly symmetric, while values of $Q \sim 0.5$ are considered highly-asymmetric. As Q varies, different attractors arise, manifest by the left and right vocal folds oscillating at different frequencies. Figure 2 shows the temporal history of the left and the right vocal fold oscillations and the minimal glottal area for $p_s = 1.392$ kPa and $Q = 0.539$ with the BLEAP flow solver. Initial conditions for this, as well as all other simulations, are given by

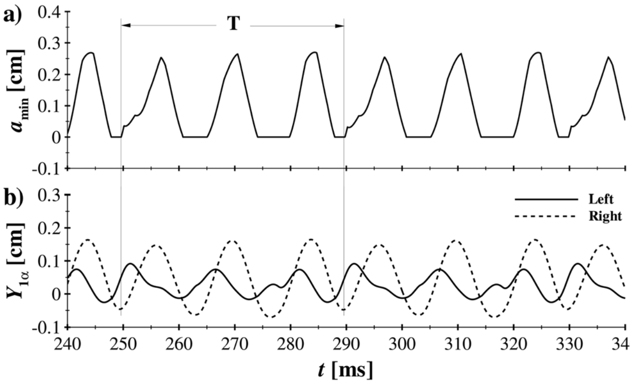

FIG. 2. Temporal evolution of (a) the minimal glottal area and (b) Y_{1L} (—) and Y_{1R}(- - -) with the BLEAP flow solution for $p_s = 1.392$ kPa and $Q = 0.539$. Over the oscillation period (T) there are three peaks in the oscillations of the right mass and four peaks in the oscillations of the left mass.

$$Y_{1\alpha}(0) = \dot{Y}_{1\alpha}(0) = 0.1, \quad Y_{2\alpha}(0) = \dot{Y}_{2\alpha}(0) = 0.0. \tag{10}$$

The coupling between the right and the left vocal fold oscillations is quantified by finding the fundamental period (T) of $a_{\min}$ [see Fig. 2(a)] by performing a correlation of the final 100 ms of the $a_{\min}$ signal with the same $a_{\min}$ signal over the range of $200 < t < 600$ ms. The period T is determined by computing the spacing between the peaks in the correlation function that are at least 99% of the maximum peak. The number of peaks in $Y_{1\alpha}$ over the period T is defined as ϕ_α. In Fig. 2 there are three peaks in the right vocal fold cycle ($\phi_R = 3$), and four peaks in the left vocal fold cycle ($\phi_L = 4$) [see Fig. 2(b)]. If T is not stationary over the correlation function, or if there are no peaks in the correlation function within 99% of the dominant peak, it is determined that $a_{\min}$ exhibited no repeating pattern (NRP). The right to left oscillation ratio, (Φ), is quantified according to

$$\Phi = \begin{cases} \dfrac{\phi_{1R}}{\phi_{1L}} & \text{for} \quad \dfrac{\phi_{1R}}{\phi_{1L}} < 1.0 \\ \phi_{1R} & \text{for} \quad \dfrac{\phi_{1R}}{\phi_{1L}} = 1.0 \\ 0 & \text{for} \quad \text{no repeating pattern (NRP)} \end{cases} \tag{11}$$

giving a ratio of 3:4 in Fig. 2.

The impact of the BLEAP scheme on the chaotic nature of the 2MM vocal fold oscillations is assessed by applying the nonlinear dynamics detection method proposed by Barahona and Poon,[1] and repeated in Tao and Jiang,[28] for time series analysis. While this method can produce spurious results in the presence of colored noise, it provides a direct correlation with the maximum Lyapunov exponent for noise-free deterministic systems, as is employed here. A time series s_n with $n = 1, \ldots, N$ in multiples of the sampling time τ can be expressed as a Volterra-Weiner-Korenberg series with degree δ and embedding dimension κ in order to predict a time series $\tilde{s}_n$, as

$$\begin{aligned} \tilde{s}_n &= e_0 + e_1 s_{n-1} + e_2 s_{n-2} + \cdots + e_\kappa s_{n-\kappa} + e_{\kappa+1} s_{n-1}^2 \\ &\quad + e_{\kappa+2} s_{n-1} s_{n-2} + \cdots + e_{\Lambda-1} s_{n-\kappa}^{\delta} = \sum_{\lambda=0}^{\Lambda-1} e_\lambda q_\lambda(n), \end{aligned} \tag{12}$$

where the coefficients e_λ are found using a Gram-Schmidt reorthonormalization approach. The total dimension of the predictive time series is $\Lambda = (\kappa + \delta)!/(\kappa!\delta!)$. The nonlinearity of the time series is now found by determining the predictive capability of $\tilde{s}_n$ by searching for the optimum values of κ, d for both linear ($\delta = 1$) and nonlinear ($\delta > 1$) combinations that minimize the information criterion

$$C(r) = \log \epsilon(r) + \frac{r}{N}, \tag{13}$$

where ϵ is the one-step-ahead prediction error given by Barahona and Poon[1] and r is the total number of polynomial terms from the truncated Volterra-Weiner-Korenberg series for any combination of (κ, δ) with $r \in [1, \Lambda]$. Chaotic behavior in the original time series is revealed if the best nonlinear model C_{nl}, obtained with $\delta > 1$, is more predictive than the linear model C_{lin}, obtained with $\delta = 1$. This occurs when $C_{\text{nl}} < C_{\text{lin}}$ for values of $r > \kappa$. Failure to meet the above criteria implies the signal is either not chaotic, or that any chaotic component is too weak to be statistically determined.[28]

The optimal value of the time lag, τ, is found for each time series by using both the method of mutual information[9] as well as investigating the graphical time-delay behavior of each series.[17] The embedding dimension κ is chosen based on the convergence of the correlation integral according to the recommendations by Theiler,[31] as well as the expected behavior of Eq. (13) for deterministic data.

III. RESULTS

The vibratory behavior of the SH 2MM is investigated by performing a parametric variation in the $Q - p_s$ plane. A reproduction of the original SH regime plot is presented in Fig. 3(a), with the initial conditions specified in Eq. (10). The regime map is generated by plotting 101 points of each variable such that $\Delta p_s = 0.003$ kPa and $\Delta Q = 0.003$. When $\Phi > 3$, the number of peaks within a repeating cycle of $a_{\min}$ is > 3, and can be as high as 30. Domains demarcated by red denote long tori and/or chaotic behavior in the vocal fold dynamics, whereas $\Phi = 0$ (blue) indicates NRP in $a_{\min}$ over the investigated time length. For some of the larger regions, values for Φ are indicated. The relatively coarse resolution of Φ (chosen for plotting visualization purposes) prevents identification of all of the unique regions of oscillation ratios. For a more detailed description, see Steinecke and Herzel.[25] The original work of SH identified a variety of nonlinear phenomena including period doubling and tripling, subharmonic regimes, and bifurcations arising from multiple attractors. For a few limited scenarios, chaotic behavior was also observed.[25] However, all of the nonlinear behavior was restricted to low symmetry values ($0.5 < Q < 0.6$) and high subglottal pressures ($p_s > \sim 0.12$), which are generally outside of the realm of even the worst pathological cases.

A $Q - p_s$ regime map implementing the BLEAP flow solution is shown in Fig. 3(b) over the expanded domain of $0.5 < Q < 0.8$ and $0.6 < p_s < 1.5$ kPa with oscillation ratios plotted as Φ. The resolution is $\Delta p_s = 0.009$ kPa and $\Delta Q = 0.009$. The dashed box demarcates the domain of the original SH plot [Fig. 3(a)]. Regions of long transients ($\Phi = 0$-NRP), multiple period oscillations ($0 < \Phi \leq 3$), and apparent chaotic behavior ($\Phi > 3$) are observed. In contrast to the SH plot, this behavior occurs over an expanded domain, with nonlinear behavior occurring at subglottal pressures that are encountered during normal speech (0.3 – 1.0 kPa).[26] Furthermore, it appears that long transients in the solution and chaotic behavior are much more prevalent in the vocal fold dynamics. Boundaries indicating transition from one oscillatory regime to another are not as clearly demarcated as in Fig. 3(a), either. The following sections quantify the nonlinear behavior of vocal fold dynamics that arise when the more realistic BLEAP flow solver is implemented.

The prevalence of nonlinear phenomena is investigated by plotting one-parameter bifurcation diagrams of the maxima of Y_{1L} for constant subglottal pressures of $p_s = 0.654$, 0.933, and 1.311 kPa, in Figs. 4(a)–4(c), respectively. The three subglottal pressures at which the bifurcation diagrams

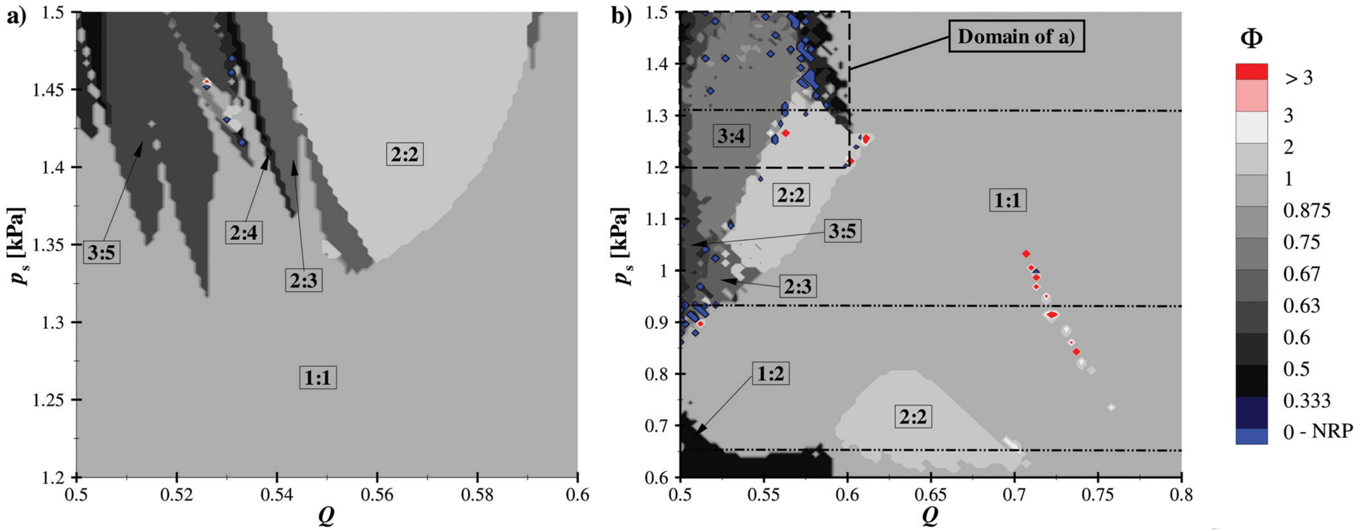

FIG. 3. (Color) Regime plot of two-parameter bifurcations in the $Q-p_s$ plane, with different attractors demarcated by Φ as specified in Eq. (11). (a) Regime plot from SH (Ref. 25) with the symmetric Bernoulli flow solver. (b) Regime plot with the BLEAP flow solver. Subglottal pressures at which the bifurcation diagrams of Fig. 4 are plotted are also shown as three lines (- .. -) at $p_s = 0.654$ kPa, $p_s = 0.933$ kPa, and $p_s = 1.311$ kPa.

are plotted are demarcated as three horizontal lines (- .. -) in Fig. 3(b). Bifurcation diagrams are created by plotting the maximum amplitude of Y_{1L} over multiple oscillations at each symmetry parameter. Single and multiple period oscillations appear as single or multiple points for each symmetry parameter, respectively, while chaotic oscillations are evidenced by vertical bands with no discernible grouping of the points. Multiple period oscillations are evident for a variety of symmetry parameters, with bifurcations in the oscillatory regime occurring as a function of the symmetry parameter, Q. The coexistence of solutions is observed by varying the initial conditions $Y_{1\alpha}$ and $Y_{2\alpha}$ for a fixed subglottal pressure and symmetry parameter. Figure 5 demonstrates the existence of 2 attractors for a constant subglottal pressure ($p_s = 0.654$ kPa) and symmetry parameter ($Q = 0.524$). This parameter set is next to a bifurcation where the vocal fold dynamics transition from one distinct vibratory pattern to another [See Figs. 3(b) and 4(a)]. While only one location is shown for brevity, the coexistence of solutions is observed for many parameter sets that coincided with bifurcations in the oscillation ratio. In contrast to the behavior produced by the Bernoulli flow solver [Fig. 3(a)] these nonlinear phenomena occur at significantly lower subglottal pressures, and persist for significantly higher values of Q. For $p_s = 0.933$ and 1.311 kPa, the bifurcation maps [Figs. 4(b) and 4(c)] exhibit complicated regimes of chaotic behavior, evidenced by vertical bands in the figure. Once the stable regime of 1:1 oscillations is reached for sufficient values of Q, the vocal fold dynamics

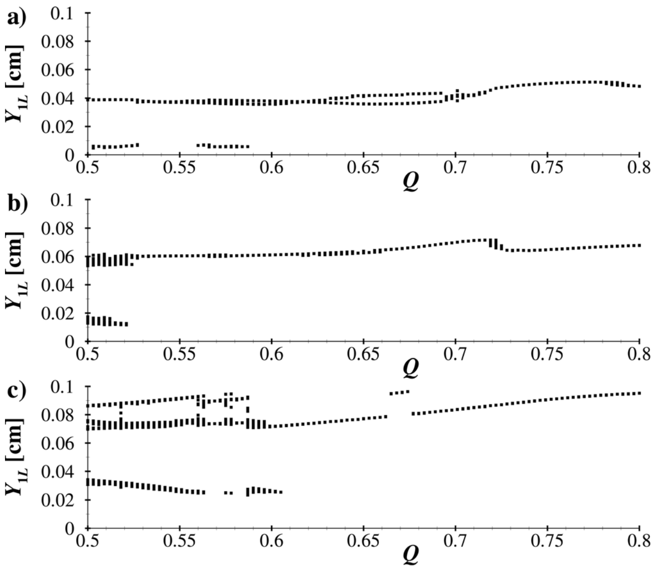

FIG. 4. Bifurcation diagrams of the maximum peaks of Y_{1L} as a function of Q at (a) $p_s = 0.654$ kPa, (b) $p_s = 0.933$ kPa, and (c) $p_s = 1.311$ kPa. See Fig. 3(b) for the location of the bifurcation diagrams with respect to the regime map.

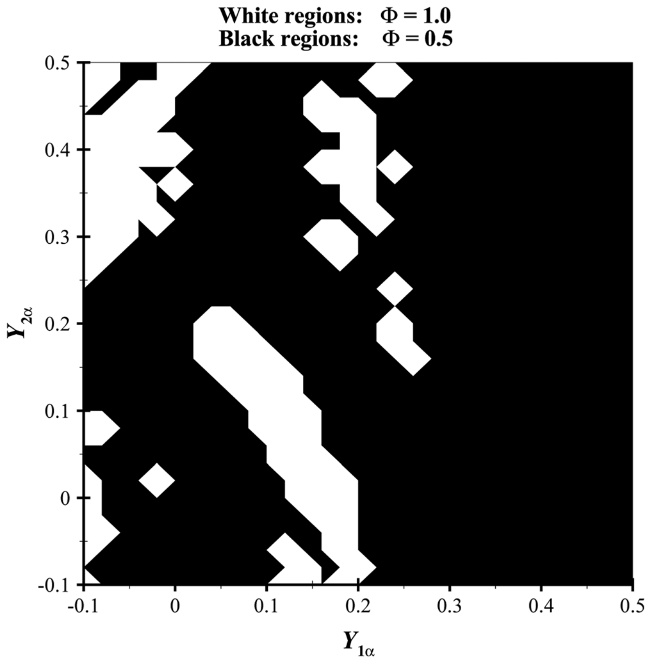

FIG. 5. Basins of attractors at $p_s = 0.654$ kPa and $Q = 0.524$ as a function of initial conditions, $Y_{1\alpha}$ and $Y_{2\alpha}$.

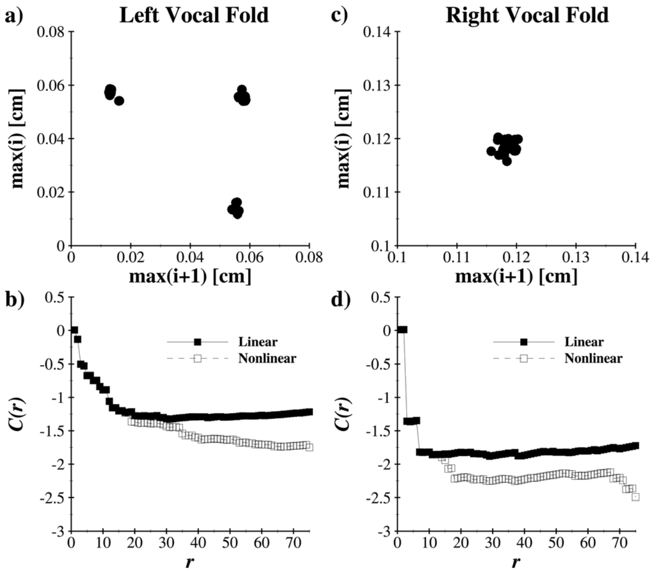

FIG. 6. Next-maximum plots (a) and (c) and $C(r)$ values as a function of the polynomial terms, r, (b) and (d) at $p_s = 0.933$ kPa and $Q = 0.512$ for Y_{1L} and Y_{1R}. Values for the time lags and embedding dimensions are $\tau_L = 65$, $\kappa_L = 12$ and $\tau_R = 40$, $\kappa_R = 15$, respectively.

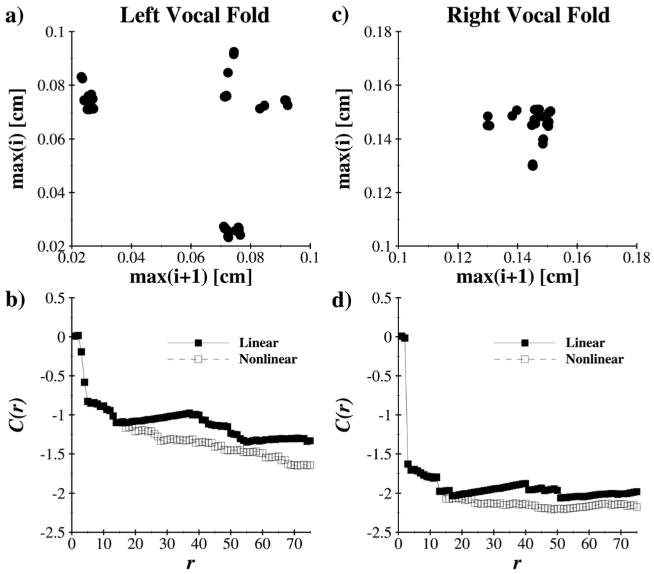

FIG. 7. Next-maximum plots (a) and (c) and $C(r)$ values as a function of the polynomial terms, r, (b) and (d) at $p_s = 1.311$ kPa and $Q = 0.587$ for Y_{1L} and Y_{1R}. Values for the time lags and embedding dimensions are $\tau_L = 54$, $\kappa_L = 13$ and $\tau_R = 56$, $\kappa_R = 13$, respectively.

are decidedly stable. This behavior is very similar to the high-level CFD-based investigations of Tao and Jiang who reported rich dynamical behavior at $p_s = 1.0$ kPa for symmetry values less than ~0.6, with 1:1 VF oscillations at higher values.[28] However, an exception to the stable behavior at larger values of Q occurs when $Q \sim 0.72$ in Fig. 4(b), and is evidenced by a band of nonlinear behavior in Fig. 3(b).

The occurrence of chaotic vocal fold motion arising from asymmetric intraglottal flow, modeled by the BLEAP solution, is investigated by performing the nonlinear detection methods discussed in Tao and Jiang,[28] and presented in Sec. II B. The nonlinear behavior of the vocal fold dynamics is reported for four cases. The first case, presented in Fig. 6 is for $p_s = 0.933$ kPa and $Q = 0.512$. This location falls within the 2:3 regime of Fig. 3(b), although it is surrounded by areas of NRP. While the algorithm for determining oscillation ratios identifies two oscillations of the right vocal fold for every three oscillations of the left, the next maximum plot of Fig. 6(b) for the right vocal fold reveals that the two points are close enough together, and there is such a high degree of variability in the peak amplitude, that it is difficult to distinguish any pattern. In contrast, the three peaks of the left vocal fold cycle, shown in Fig. 6(a), are easily identified, although there is still variability from cycle to cycle. Plots of the linear and nonlinear polynomial terms in Figs. 6(b) and 6(d) indicate chaos in the left and the right vocal fold motions, because the nonlinear polynomial terms are significantly more predictive.

In Fig. 7 the nonlinear dynamics of the vocal fold oscillations are reported at $p_s = 1.311$ kPa and $Q = 0.587$, where the left to right oscillation peaks were found to be 8:11. In Fig. 3(b) this point is located between regions of 2:2 and 1:1 oscillations, where the boundary exhibits significant variability, albeit a "stable" oscillation ratio is found. The next maximum-plots of Fig. 7 exhibit a pattern of maximum peaks that is difficult to distinguish. As is expected, the nonlinear polynomial is also more predictive than the linear polynomial, indicating the presence of chaotic vocal fold motion along the region between two seemingly stable oscillation ratios in the regime plot of Fig. 3(b). This is similar to the findings of Tokuda *et al.* regarding the presence of chaotic regimes at the interface of two attractors.[34]

Vocal fold behavior in regions of NRP, colored blue in Fig. 3, is represented in Fig. 8 for $p_s = 1.311$ kPa and $Q = 0.563$. In these regions, the oscillation ratio algorithm is unable to find any repeating pattern in the minimal glottal area over the length of the available time series, and hence no oscillation ratio is computed. As expected, there is no discernible pattern in the next-maximum plots [Figs. 8(a) and 8(c)] and

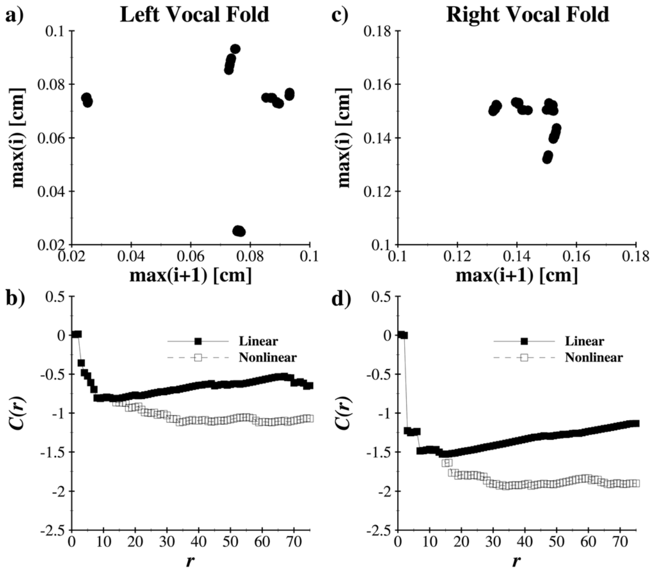

FIG. 8. Next-maximum plots (a) and (c) and $C(r)$ values as a function of the polynomial terms, r, (b) and (d) at $p_s = 1.311$ kPa and $Q = 0.563$ for Y_{1L} and Y_{1R}. Values for the time lags and embedding dimensions are $\tau_L = 61$, $\kappa_L = 13$ and $\tau_R = 56$, $\kappa_R = 12$, respectively.

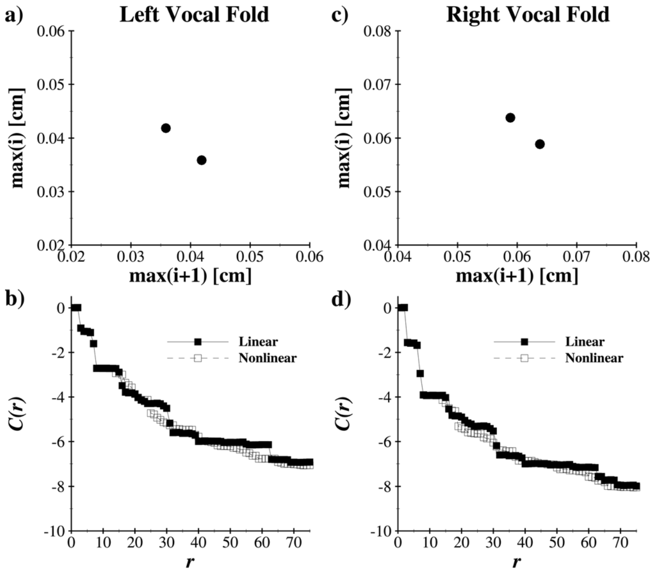

FIG. 9. Next-maximum plots (a) and (c) and $C(r)$ values as a function of the polynomial terms, r, (b) and (d) at $p_s = 0.654$ kPa and $Q = 0.653$ for Y_{1L} and Y_{1R}. Values for the time lags and embedding dimensions are $\tau_L = 56$, $\kappa_L = 12$ and $\tau_R = 56$, $\kappa_R = 12$, respectively.

the nonlinear polynomial curves in Figs. 8(b) and 8(d) is the most predictive, indicating chaos in the vocal fold dynamics.

Figure 9 shows the nonlinear analysis results of the vocal fold oscillations for $p_s = 0.654$ kPa and $Q = 0.653$; a region of stable 2:2 oscillation ratio in Fig. 3(b). The next maximum plots [Figs. 9(a) and 9(c)] indicate a bimodal pattern of cycle-to-cycle amplitude variation for both the left and the right vocal folds, although the amplitudes differ between each side. Variations in the peak amplitudes vary by less than ~1.5% of the peak amplitude. Similarly, the linear and nonlinear polynomial plots of $C(r)$ [Figs. 9(b) and 9(d)] do not predict chaotic motion.

IV. DISCUSSION AND CONCLUSIONS

The initial $Q - p_s$ regime plot proposed by SH indicates nonlinear phenomena for values of p_s well above the range of "normal" phonation, and for excessive tension asymmetries.[26] Implementation of the more physically-realistic BLEAP scheme in the 2MM of SH results in the onset of chaotic behavior in the vocal fold dynamics at much lower values of subglottal pressure, and for more symmetric tissue properties. It is interesting to note that for values of $Q > \sim 0.76$, ordered vocal fold oscillations occur with 1:1 oscillation ratios. These results suggest that the development of asymmetric flows within the glottis during "normal" phonation, where there are small tension and geometric imbalances between the vocal folds, do not influence the dynamics of speech significantly. However, in pathological voice, where tension imbalance may be more significant due to paralysis or degeneration, asymmetric flows have a pronounced detrimental effect on speech quality. This behavior is consistent with recent clinical investigations of speech where small asymmetries appear to be well tolerated by the general population with little impact on voice quality,[24] but large asymmetries like those found in SLN result in vocal fold motion that has been described as *gegenschlagen*,[20] or "dashing-against-each-other". In this scenario the glottal space does not remain aligned with the glottal midline, and the voice quality is severely affected.[19]

Modeling asymmetric glottal flows and imbalanced vocal fold tension with the BLEAP scheme results in the emergence of chaotic behavior within the range of normal speech. This behavior is very similar to that previously reported by Tao and Jiang[28] and further expands their findings. It appears to be especially sensitive along borders of varying oscillation ratios, regions where a large number of oscillations are needed to produce a repeating pattern in $a_{\min}$, and in regions of NRP. These findings are consistent with recent observations that the onset of chaos often occurs at register transitions in voice.[34,36] However, care should be taken in labeling entire regions as "chaotic" since the relatively few investigative points prevent a comprehensive delineation of chaotic and non-chaotic behavior over the broad parameter space, as evidenced by the periodic behavior in Fig. 9. The advantage of the current BLEAP method over fully-coupled CFD flow solvers is the ability to accurately model the complex vocal fold dynamics with a simple algebraic solution that is easily implemented into existing 2MM of speech without any added computational cost.

Based on their results obtained with a coupled CFD flow solver and the SH 2MM of speech, Tao and Jiang proposed that the onset of chaos in vocal fold dynamics is most likely due to asymmetric flow attachment arising due to formation of the Coanda effect within the glottis, although it was also proposed that other factors such as unsteady flow separation, vortex shedding and turbulence may also contribute to this behavior.[28] By only capturing asymmetric flow attachment and not accounting for higher order effects, implementation of the BLEAP scheme into the SH 2MM of speech demonstrates that the Coanda effect is a dominant contributor to the onset of chaotic vocal fold motion in tension imbalanced speech. Nevertheless, the inability of the BLEAP scheme to model higher-order fluid dynamics effects such as vortex shedding and turbulence suggests that the regime map of Fig. 3(b) is most likely a conservative estimate of nonlinear phenomena that would be expected to occur during tension imbalanced speech.

The ease with which the BLEAP scheme is implemented into existing multi-mass speech models facilitates a wide range of feasible studies that can be performed in order to investigate the impact of the more physically-relevant flow solver on pathological speech; including recurrent laryngeal nerve paralysis,[25] Parkinsonian speech,[23,39] and vocal tremor,[23] to name a few.

The current investigation has neglected the role of acoustic coupling during voiced speech; that is, the idea that acoustic pressures create large resonances within the vocal tract, which in turn act as a feedback loop and impact vocal fold dynamics due to modulation of the subglottal and supraglottal pressure field.[32,37] The inclusion of acoustic coupling in the BLEAP investigations, which is an avenue of research currently being pursued, is expected to magnify the impact of the BLEAP flow solver on the vocal fold dynamics and more importantly, the radiated sound field.

ACKNOWLEDGMENTS

This work was supported in part by NSF Grant #CBET-1036280. The authors would like to thank Dr. Maurizio Porfiri for his insightful comments regarding the preparation of the manuscript.

[1] M. Barahona, and C. Poon, Nature (London) **381**, 215 (1996).
[2] J. S. Drechsel and S. L. Thomson, J. Acoust. Soc. Am. **123**, 4434 (2008).
[3] B. D. Erath, S. D. Peterson, M. Zañartu, G. R., Wodicka, and M. W., Plesniak, J. Acoust. Soc. Am. **130**, 389 (2010).
[4] B. D. Erath, and M. W. Plesniak, Exp. Fluids **40**, 683 (2006).
[5] B. D. Erath, and M. W. Plesniak, Exp. Fluids **41**, 735 (2006).
[6] B. D. Erath and M. W. Plesniak, Exp. Fluids **49**, 131 (2010).
[7] B. D. Erath, and M. W. Plesniak, Int. J.Heat Fluid Flow **31**, 468 (2010).
[8] B. D. Erath and M. W. Plesniak, J. Acoust. Soc. Am. **129**, EL64 (2011).
[9] A. M. Fraser and H. L. Swinney, Phys. Rev. A **33**, 1134 (1986).
[10] A. G. Hansen, *Similarity Analyses of Boundary Value Problems in Engineering*, (Prentice-Hall, New Jersey, 1964), pp. 1–30.
[11] H. Herzel, D. Berry, I. R. Titze, and I. Steinecke, Chaos **5**, 30 (1995).
[12] J. J. Jiang and Y. Zhang, J. Acoust. Soc. Am. **112**, 2127 (2002).
[13] J. J. Jiang, Y. Zhang, and C. N. Ford, J. Acoust. Soc. Am. **114**, 2198 (2003).
[14] J. J. Jiang, Y. Zhang, J. MacCallum, A. Sprecher, and L. Zhou, Folia Phoniatr. Logop. **61**, 342 (2009).
[15] J. J. Jiang, Y. Zhang, and C. McGilligan, J. Voice **20**, 2 (2006).
[16] J. J. Jiang, Y. Zhang, and J. Stern, J. Acoust. Soc. Am. **110**, 2120 (2001).
[17] H. Katz and T. Schreiber, *Nonlinear Time Series Analysis* (Cambridge University Press, Cambridge, 2004), pp. 36–41.
[18] M. H. Krane, M. Barry, and T. Wei, J. Acoust. Soc. Am. **122**, 3659 (2007).
[19] A. H. Mendelsohn, M. W. Sung, G. S. Berke, and D. K. Chhetri, Ann. Otol. Rhinol. Laryngol. **116**, 85 (2007).
[20] D. M. Moore, B. R. Gerrat, R. R. Karin, and G. S. Berke, Laryngoscope **97**, 543 (1987).
[21] X. Pelorson, A. Hirschberg, A. P. J. Wijnands, and H. M. A. Bailliet, J. Acoust. Soc. Am. **96**, 3416 (1994).
[22] R. C. Scherer, D. Shinwari, K. J. DeWitt, C. Zhang, B. R. Kucinschi, and A. A. Afjeh, J. Acoust. Soc. Am. **109**, 1616 (2001).
[23] J. Shao, J. K. MacCallum, Y. Zhang, A. Sprecher, and J. J. Jiang, J. Commun. Disord. **43**, 35 (2010).
[24] H. S. Shaw, and D. D. Deliyski, J. Voice **22**, 23 (2008).
[25] I. Steinecke and H. Herzel, J. Acoust. Soc. Am. **97**, 1874 (1995).
[26] K. N. Stevens, *Acoustic Phonetics* (MIT, Cambridge, MA, 1998) pp. 27–37.
[27] J. Suh and S. Frankel, J. Acoust. Soc. Am. **121**, 3728 (2007).
[28] C. Tao, and J. J. Jiang, Phys. Rev. E **77**, 061922 (2008).
[29] C. Tao and J. J. Jiang, Chaos **19**, 023113 (2009).
[30] C. Tao, Y. Zhang, D. G. Hottinger, and J. J. Jiang, J. Acoust. Soc. Am. **122**, 2270 (2007).
[31] J. Theiler, Phys. Rev. A **34**, 2427 (1986).
[32] I. R. Titze, J. Acoust. Soc. Am. **123**, 2733 (2008).
[33] I. Tokuda and H. Herzel, Chaos **15**, 013702 (2005).
[34] I. Tokuda, J. J. Horacek, J. G. Svec, and H. Herzel, Chaos **18**, 013102 (2008).
[35] P. Yu, R. Garrel, R. Nicollas, and M. Ouaknine, Folia Phoniatr. Logop. **59**, 20 (2007).
[36] M. Zañartu, D. D. Mehta, J. C. Ho, G. R. Wodicka, and R. E. Hillman, J. Acoust. Soc. Am. **129**, 326 (2011).
[37] M. Zañartu, L. Mongeau, and G. R. Wodicka, J. Acoust. Soc. Am. **121**, 1119 (2007).
[38] Y. Zhang, J. J. Jiang, L. Biazzo, and M. Jorgensen, J. Voice **19**, 519 (2005).
[39] Y. Zhang, J. Jiang, and D. A. Rahn, Chaos **15**, 033903 (2005).
[40] Y. Zhang and J. J. Jiang, J. Sound Vib. **316**, 248 (2008).
[41] Y. Zhang, C. Tao, and J. J. Jiang, Chaos **16**, 023118 (2006).